Multi-Shape-Changing Interpenetrating Networks with Shape Memory Effect and Adaptive Plastic Deformations

Lin Wang[1], Shanshan Wu[2], Xing Guo[1,2], Jing Fan[3], Shaobing Zhou[2]*, Zi Chen[1,4]*

[1] Thayer School of Engineering, Dartmouth College, 03755 Hanover, New Hampshire, USA.
[2] Key Laboratory of Advanced Technologies of Materials Ministry of Education, School of Materials Science and Engineering, Southwest Jiaotong University, 610031 Chengdu, China.
[3] Department of Mechanical Engineering, City College of New York, 10031 New York, NY, USA.
[4] Division of Thoracic Surgery, Brigham and Women's Hospital, Harvard Medical School, 02115, Boston, MA, USA.

Lin Wang and Shanshan Wu contributed equally.
Correspondence and requests for materials should be addressed to zchen33@bwh.harvard.edu or shaobingzhou@swjtu.edu.cn

Abstract

Shape-changing materials with precisely programmable configurations, each having its own functional regime, provide a wide range of applications in engineering and biomedical fields. Polymers with dynamic reversible covalent/non-covalent bonding feature the potential of having remarkable plasticity, which endows them with the capability of undergoing significant and sophisticated shape changes. Here we report a facile method to build an interpenetrating network (IPN) structure with plastic deformation and shape memory properties. The IPN is consisting of Poly(vinyl Alcohol) (PVA) with slight chemical covalent crosslinking and poly(UPyMA-AAc) with two potential dynamic reversible non-covalent bonding (quadruple hydrogen-bonding and ferric coordination bonding). This IPN structure not only has the capability of thermal plasticity and metal-coordinated plasticity, but also possesses shape memory properties similar to typical shape memory polymers. Hence, the polymers with this structure can undergo programmable shape changes through sequential adaptive plastic deformations triggered by a variety of stimuli.

Keywords: plastic deformation, interpenetrating network, shape changing, cumulative plastic transition, reversible noncovalent bonding

1. Introductions

Shape changing behaviors in response to external environmental stimuli are pervasive in nature.[1, 2] Stimuli-responsive shape changing polymers (SCPs) have gained increasing attention in various technological applications, such as intelligent sensors,[3] robotics,[4] and biomedical devices.[5] In advancing these technologies, it is necessary to examine and mimic the complicated and diverse shape changing behaviors of natural systems. Among SCPs, shape memory polymers (SMPs), which is capable of fixing a temporary programmed shape and later recovering its permanent structure on demand, have been widely studied in recent years.[6] Dual-shape memory polymers can memorize a programmed temporary shape by switching the system from one state to the other. Various molecular relaxations and phase transitions, e.g., vitrification, crystallization, or reversible noncovalent bond interactions, can be employed to fix the temporary shape. Therefore, a combination of various mechanisms, when appropriately employed, can create multi-shape memory polymers.[7, 8] In the recently discovered thermadapt polymers, the programmed shape, i.e., the ultimate structure after all shape changing processes, does not recover its initial shape when subjected to external stimuli, thus enabling the design of highly complicated permanent 3D shapes without using any molds. The permanent 3D shapes are achieved by the rearrangement of molecular switch in thermadapt polymer, such as reversible covalent or noncovalent bonding.[9-14] Regarding the fundamental mechanism, the shape memory property of most SMPs results from their inherent entropic elasticity, more specifically, there are at least two parts in the traditional shape memory polymers. The first part is the elastic segment of polymer, which is called the elastic part. After programming either at high or low temperatures, the elastic part stores elastic energy. The second part is the soft segment, known as the transition part. The transition part provides constraint to prevent shape recovery at low temperatures. Only reheating to soften the transition part can remove the constraint and, thus driven by the stored elastic energy in the elastic part, the polymer returns to its original shape.[15-17] By contrast, the shape changing property of

thermadapt materials is based on the plastic deformation that can be achieved by dynamic covalent or non-covalent bond exchange in their polymer network.[18-20] Moreover, the shape-programming behavior of thermadapt polymers is predictable, repeatable, and can also be accumulative, i.e., the shape at a later stage can be obtained by the plastic deformation from the previous stage.[21]

The discovery of thermadapt polymers with plasticity has filled the gap in self-adaptive smart systems. By introducing dynamic covalent or non-covalent bond to the SMPs structure, the resultant thermadapt SMPs structure has both plasticity and shape memory properties. The plastic deformation in smart materials has been realized using the reversible interaction of Diels-Alder,[22] transesterification,[16] diselenide bond,[19] transcarbamoylation,[23] quadruple hydrogen bonding[24, 25] and metal-coordination.[26] Among these reversible dynamic covalent and non-covalent bonding, quadruple hydrogen bonding and metal-ligand bonding have attracted more attention due to their good switchability. The bonding strength in the two types mentioned above rivals that of traditional noncovalent bonds.[27, 28] Thereby the materials containing the two types of bonding have malleability, self-healing, shape memory properties.[10, 29] For instance, ureidopyrimidone (UPy) dimers exhibit highly dynamically reversible response when subjected to a change in temperature or exposed to different solvents induced by the transition between dissociation and reconfiguration.[30-34] Among the metal coordination bonding, ferric (Fe^{3+}) is usually used with poly(acrylic acid) (PAA) to structure the metal-ligand coordination network due to the ionic interaction between Fe^{3+} and carboxyl groups.[35-37]

Recently, double networks that contains two distinct dynamic transition units in one system have been extensively investigated in tough hydrogels and self-healing fields.[37-39] Interpenetrating networks (IPNs) have gained tremendous attention owing to the significant improvement of its properties in mechanical and other aspects.[40] Although significant progress in plastic deformation of SMP has been achieved, there also remains a long-standing

challenge, i.e., how to fabricate smart systems with multiple transition means that can undergo a series of plastic deformations under various environmental stimuli.

Here we aim to achieve the multi-shape changing and adaptive plastic deformation in a smart system that also exhibit shape memory capability. To tackle this problem, we designed an IPN structure which contains slight crosslinked poly(vinyl alcohol) (c-PVA) and poly(ureidopyrimidone methacrylate-co-acrylic acid) (poly(UPyMA-AAc)) with dynamic non-covalent bonding, which is the first time for such structure to be realized to the authors' knowledge. Because the IPN has an interlaced structure on the molecular scale, there must be two or more components in IPN which are neither covalently bonded nor separated. We chose PVA, which has become one of the most commonly used polymers to generate IPNs with acrylic monomers because of its good hydrophilicity and biocompatibility.[41] The IPN structure features good shape memory, thermal plastic deformation, and metal coordination properties based on its unique structure. The IPN underwent plastic deformation by virtue of the formation of the UPy dimers and ferric coordination bonding. Besides, the Post-Plasticity-Transition IPN (PPT-IPN) has a notable shape memory effect. We further demonstrated that adaptive plastic deformations of IPN (after thermal stimulation) occurs when immersed into ferric solution and EDTA solution consequtively. Furthermore, negligible deterioration in the shape retention ratio of the PPT-IPN was observed after treatment by ferric/EDTA solutions in several cycles. In a broader sense, the IPN system developed here will fall under the category of vitrimer and the most features reported here can be achieved by vitrimer, [42] or vitrimer-like materials.[43, 44] The IPN structure containing those two types of non-covalent crosslinking exhibited both shape changing effect and continuous adaptive plastic deformation, so this new method paves the way for the development of next-generation shape-programmable and reconfigurable devices.

2. Methods

2.1. Materials.

2-Amino-4-hydroxy-6-methylpyrimidine (98%), hydrochloric acid (HCl), Polyvinyl alcohol (PVA with saponification degree of 99% and polymerization degree of 1700) and 2,2'-azobis(isobutyronitrile) (AIBN) were purchased from Sigma-Aldrich. 2-isocyanatoethyl methacrylate was purchased from TCI America. Glutaraldehyde (GA, 50 wt% aqueous solution) and acrylic acid were purchased from Alfa Aesar. Ferric chloride was purchased from EMD Millipore Corporation. AIBN was recrystallized from ethanol. All other chemicals were used as received.

2.2. Synthesis of Ureidopyrimidone Methacrylate (UPyMA).

UPyMA was synthesized using the method described in Reference [30]. 2-Amino-4-hydroxy-6-methylpyrimidine was completely dissolved in DMSO in an oil bath at 150 °C, then quickly placed into water bath at room temperature (RT). 2-isocyantoethyl methacrylate was added immediately and reacted at room temperature for 30 min. The precipitated white solid was washed with hexane three times and dried in a vacuum oven for 1 day. The resultant UPyMA monomer can dissolve in DMSO, DMF and $CHCl_3$, however, it is insoluble in acetone, water, or ethanol. The chemical structure of UPyMA was confirmed by ^{1}H-NMR. Figure S2 shows the ^{1}H-NMR spectrum of UPyMA. ^{1}H-NMR (500 MHz, $CDCl_3$) ppm: 13.0 (g, 1H, -NH-C(CH_3)=), 11.9 (h, 1H, -NH-C=N-), 10.5 (f, 1H, -NH-C=O-), 6.3 (i, 1H, -CH=C(CH_3)-), 5.8 (a, 1H, $CH_{(cis)}$=C(CH3), 5.5 (b,1H, $CH_{(trans)}$=C(CH_3)), 4.3 (d, 2H, -COOCH_2-), 3.6 (e, 2H, CH_2NHCO-), 2.3 (j, 3H, -NHC(CH_3)=CHCO-), 1.9 (c, 3H, CH_2=C(CH_3)).

2.3. Synthesis of Poly(ureidopyrimidone methacrylate-co-acrylic acid) (Poly(UPyMA-AAc)).

Poly(UPyMA-AAc) was synthesized in DMF with AIBN as the initiator under a nitrogen atmosphere via free radical copolymerization. Specifically, UPyMA (8 $_{mol}$%) was completely dissolved in DMF at 70 °C, followed by the addition of acrylic acid (92 $_{mol}$%) and AIBN (1 wt%). The transparent solution was stirred for 24 hours at 70 °C, then precipitated in diethyl ether,and redissolved in deionized water. The resulting mixture was cooled to room

temperature, followed by dialysis against deionized water to remove unreacted monomer. The mixture was then freeze dried for 2 days. The resultant final product, poly(UPyMA-AAc), is soluable in water. Figure S3 shows the ^{1}H-NMR spectrum of poly(UPyMA-AAc). ^{1}H-NMR (500 MHz, D_2O) ppm: 12.0 (e, 1H, -COOH), 10.8~11.2 (h,i,j, -NH-), 6.0 (m, 1H, -CO-CH=C(CH_3)-), 4.2 (f, 2H, -COOCH_2-), 3.3 (g, 2H, CH_2NHCO-), 2.6 (a, 1H, -CH(COOH)-CH_2-), 2.4 (k, 3H, -NHC(CH_3)-C=C), 1.3 (d, 3H, -C(CH_3)-CH_2). The molar fraction of UPyMA and acrylic acid in the copolymer were calculated by the ratio of integral areas of UPyMA methane proton (6.0 ppm) and acrylic acid carboxyl proton (12.0 ppm), the molar ratio of UPyMA and acrylic acid is 7.5% : 92.5%, which has approximate ratio to the feeding composition. The characteristic chemical shifts and the integrated area of distinct chemical shifts in ^{1}H-NMR spectra confirmed that UPyMA and Poly(UPyMA-AAc) were synthesized successfully.

2.4. Fabrication of IPN.

Aqueous solutions of 10 weight% PVA and 10 weight% poly(UPyMA-AAc)) were mixed to form a milky-white mixture was obtained by mixing the two solutions. The pH was adjusted to 4. GA (0.5 weight% of total weight) was then added into the solution under stirring. The resultant mixture was poured into a PVDF mold, and kept at room temperature for 2 days before peeling off to form the IPN film. A series of IPN materials (Table S1 and Figure S1) were synthesized by varying the weight ratio of GA content while maintaining the overall stoichiometric balance between PVA and Poly(UPyMA-AAc) as 1:1. The selected ratio is based on the range of the glass transition temperature and the rheology property of IPN. Poly(UPyMA-AAc) has a high Tg and c-PVA has a wide glass transition temperature range. Besides, poly(UPyMA-AAc) and c-PVA films were prepared following the same procedure. Moreover, the IPN film is transparent.

2.5. Effect of GA Content on Swelling Property of c-PVA.

We investigated the effect of GA content on the crosslink density and swelling of c-PVA. As shown in Figure S9, the gel fraction of different c-PVA was calculated by Equation 1, where an increase in crosslink density was obtained due to the increasing amount of crosslinker. The corresponding swelling properties of the c-PVA tend to decrease. This is because the increase of GA content leads to the increase of the polymer rigidity, and subsequently restricts the chain mobility and reduces the free volume space.[31]

2.6. Fabrication of Ferric Ion Coordination IPN (Fe-IPN).

Firstly, IPN specimen was immersed into 0.5 mol/L $FeCl_3$ solution for 5 hours. Water on IPN surface was then wiped off. Finally, the specimen was dried in vacuum oven for 24 hours to form a black specimen.

2.7. The Absorption and Release of Ferric Ions in Water.

The IPN specimen were immersed in 0.5 mol/L $FeCl_3$, and the $FeCl_3$ solutions at different time intervals. Different concentrations of the initial solution and that after IPN absorption indicate the absorption amount of ferric ion. Dried Fe-IPN specimen was placed in water. Water was taken at different time intervals was tested to obtain the amount of cumulative release.

2.8. Adaptive Plastic deformation.

The synthesized IPN structure with two different dynamic non-covalent bonding enables it to undergo plastic deformation. The quantitative plastic deformation was tested by DMA under control force model. The material was treated by heating at 150 °C, which is above its transition temperature, for 15 min; at this temperature the material could be stretched to a large deformation by a small stress. The PPT-IPN can be obtained by cooling the deformed sample and subsequently releasing the stress. Here the plastic deformation occures due to the dissociation and reconfiguration of UPy dimers. The dynamic ferric ion coordination and de-coordination also enables the IPN to have a potential shape reconfiguration property. A flat sample were bent into an airplane shape at 70 °C, at which the UPy dimers cannot be broken,

then immersd into 0.5 mol/L $FeCl_3$ solution under stress for 5 h. The coordinated IPN was dried in a vacuum oven for 24 h to obtain a coordinated PPT-IPN. The shape memory property of PPT-IPN (UPy-and coordinated-induced) was investigated by using above mentioned methods.

2.9. The Sequential Adaptive Plastic deformation.

We studied the sequential adaptive plastic deformation of IPN under thermo and $FeCl_3$. Sequential adaptive plastic deformations were generated by exposing to a high temperature and then $FeCl_3$ solution.

3. Results

3.1. Fabrication route and Characterization of IPN.

In this work, we integrated the reversible UPy group and ferric coordination into a slightly crosslinked PVA network to form an IPN structure (Figure 1). The two types of reversible non-covalent bonding endow the IPN with the capability of continual thermal/coordination plastic deformation, as well as further reversible shape changing transition in $FeCl_3$ and EDTA solutions consecutively (Figure 1C). The chemical structures of UPyMA and poly(UPyMA-AAc) were measured by ^{1}H-NMR. The characteristic chemical shifts and the integrated area of distinct chemical shifts in ^{1}H-NMR spectra (Figure S2 and S3, Supporting Information) confirmed that UPyMA and Poly(UPyMA-AAc) were successfully synthesized. By calculating the ratio of integral areas of UPyMA methane proton (6.0 ppm) and acrylic acid carboxyl proton (12.0 ppm), the molar ratio of UPyMA and acrylic acid in poly(UPyMA-AAc) is 1 : 12.3, which is similar to the ratio in the feeding composition.

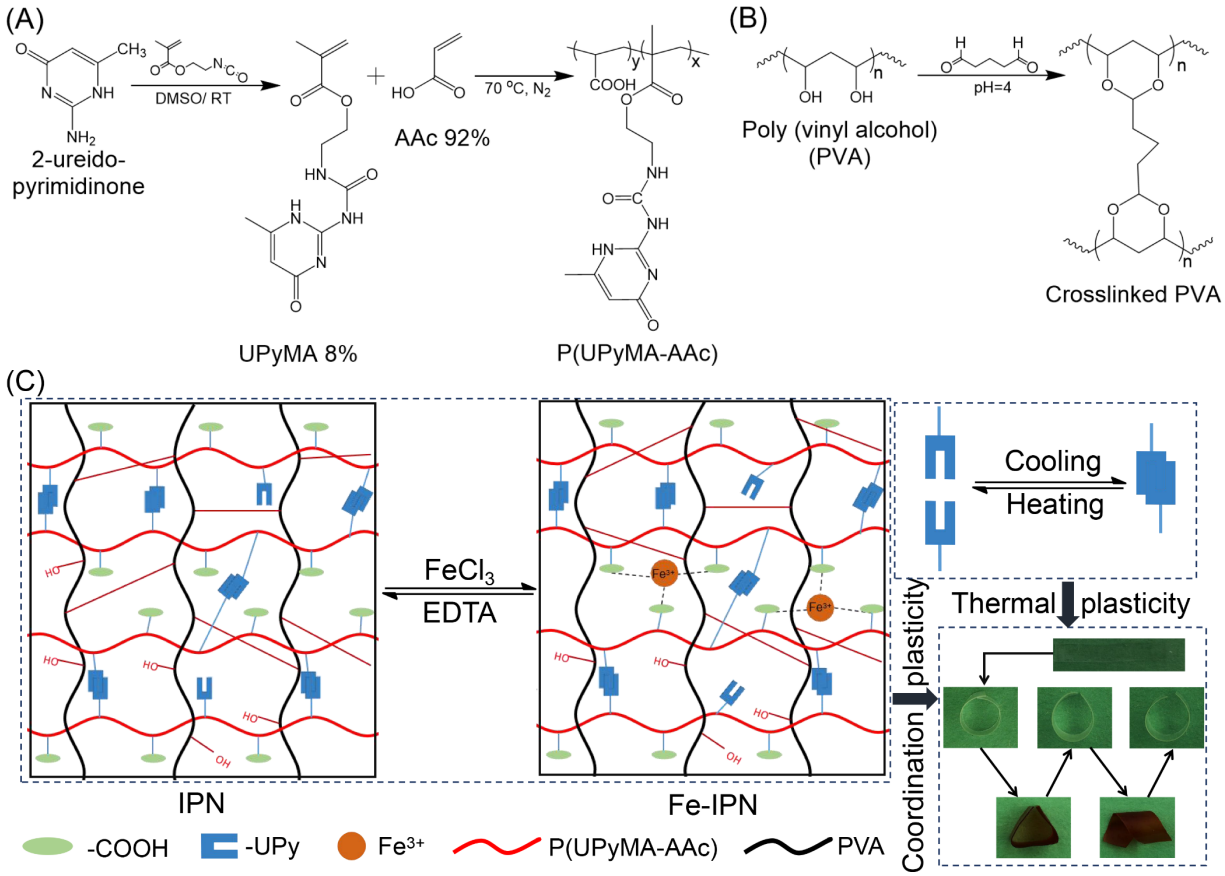

Figure. 1 The synthetic route of poly(UPyMA-AAc) (**A**) and crosslinked PVA (**B**); schematic illustrations showing the reversible transition between IPN and Fe-IPN. Besides, by integrating of two types of non-covalent bonding in IPN structure feature thermal plastic deformation and coordination plastic deformation, as well as sequential plasticity transtion. Step ① : thermal plasticity process; Step ② : coordination plasticity process; Step ③ : EDTA treatment. (**C**).

From the structural perspective, c-PVA provide a crosslinking basis that endow the IPN with elasticity, meanwhile fixing the copolymer in the IPN structure. The copolymer can also stabilize the IPN structure by forming self-complementary multiple hydrogen bonds or by ferric coordination. To verify the successful fabrication of IPN, atomic force microscope (AFM) and scanning electron microscope (SEM) images of IPN was acquired, which showed that IPN revealed a almost homogeneous morphology without obvious phase separation (Figure S4, Supporting Information). Furthermore, considering the solubility (Figure S5, Supporting Information), We found that the c-PVA with a low crosslinking degree is dispersed, rather than swelled, in water. The results of Table S1 and Figure S9 showed that the swelling degree of c-PVA with 0.5% GA content can reach up to 300% without oscillating condition, however, under oscillating condition, we found that the swelled c-PVA is broken. The storage modulus G′ and

loss modulus G″ at a small strain of 0.01% with the frequency (0.1~100 rad/s) were obtained by rheological measurement. As shown in Figure S6, when the PVA solution without crosslinking, the storage modulus G′ is smaller than loss modulus G″. In the contrast, the storage modulus G′ is larger than loss modulus G″ of the c-PVA with 0.5% GA content. It illustrated that the PVA solution became to hydrogel when the PVA solution was crosslinked. The c-PVA with 0.5% GA content exhibited some elasticity that may be attributed to its crystalline property, but showed poor shape memory property under high temperature, plastic deformation occured due to the lower crosslinking density. Poly(UPyMA-AAc) also is water-soluble. However, IPN underwent swelling instead of getting dissolved in water, further indicating the successful fabrication of IPN.

3.2. Thermal-induced Shape Memory Properties of the IPN and the Fe-IPN.

By integrating UPy dimerization and ferric coordination in one system, the Fe-IPN structured material boasted superior shape-changing properties, such as a combination of shape memory effect, thermal, coordination, and sequential plastic deformations under different stimuli. Firstly, we investigated the thermal-induced shape memory properties of IPN and Fe-IPN. To determine the shape transition temperatures of IPN and Fe-IPN, differential scanning calorimetry (DSC) and dynamic mechanical analysis (DMA) were tested. Compared to the transition temperature of c-PVA and Poly(UPyMA-AAc), there exists a wide glass transition temperature area from 50 °C to 150 °C for IPN structure and 50 °C to 170 °C for Fe-IPN, respectively (Figure S7, Supporting Information), and the glass transition temperature of Poly(UPyMA-AAc) (115 °C) in the DSC curve of IPN was disappeared, indicating the successful fabrication of IPN structures. The DMA results further showed that both the IPN and Fe-IPN possess a wide transition temperature area from about 40 °C to 100 °C

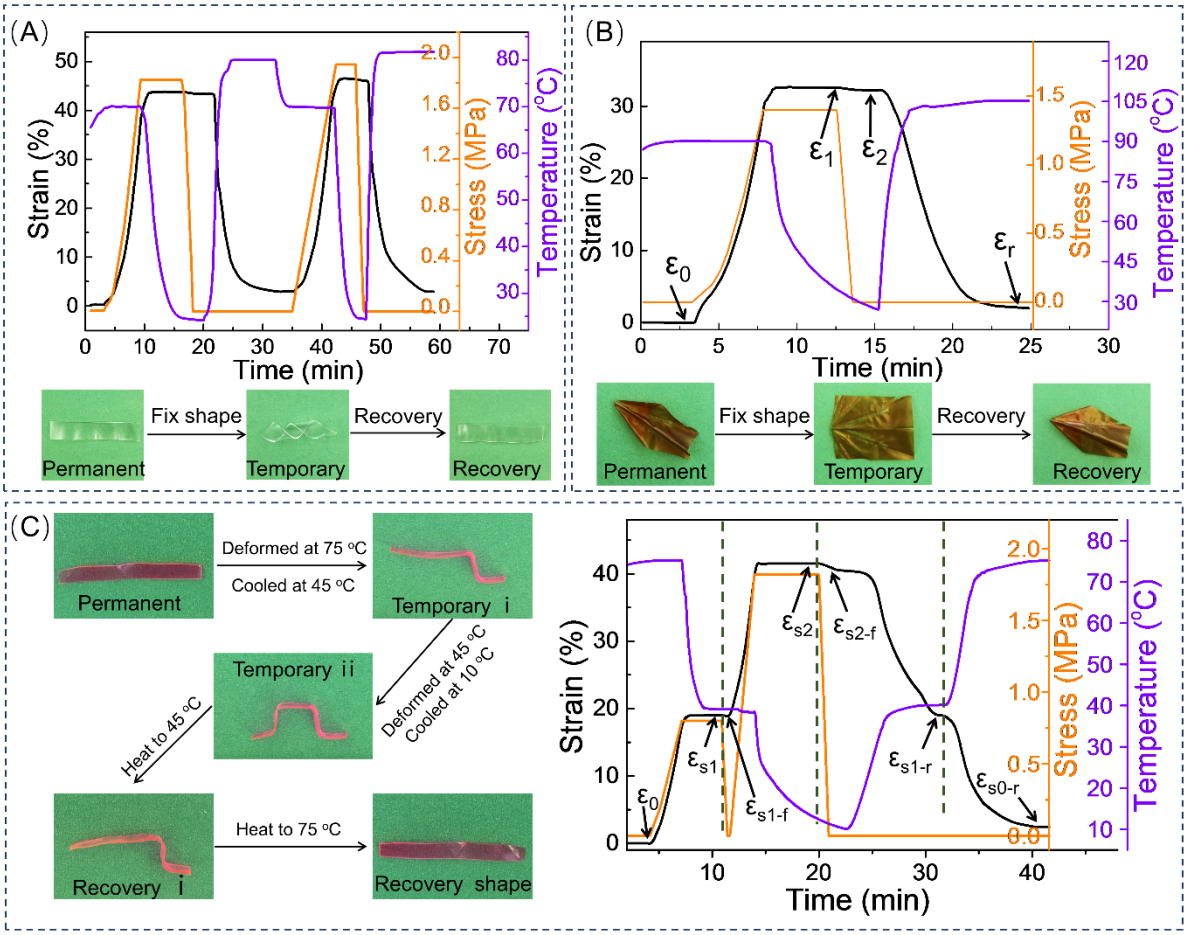

Figure. 2 Shape memory cycles of IPN (**A**) and Fe-IPN (**B**); triple shape memory fixing and recovery process (**C**).

(Figure S6B, Supporting Information). The wide transition temperature area and the significant variation in storage modulus as a function of temperature form the foundation for the potential triple shape memory property.[45, 46] Because the UPy dimers are exchangeably bonded, and the exchange rate increases as temperature elevates,[24] the IPN exhibit plasticity when treated by high temperature due to the rearrangement of the molecular chain that results in a new crosslinked structure. Meanwhile, PPT-IPN was stable at low temperature due to the stress relaxation of IPN structure upon deformation, and thus resulting in a permanent deformation.[47, 48] Then, we studied the shape memory effect of IPN. As shown in Figure 2A and Video 1, an IPN film could be deformed to a helical shape at 80 °C and the deformed shape gets fixed at room temperature (RT). The temporary helical shape was stable at RT and could recover its initial shape upon heated to an elevated temperature. From the results of DMA, the shape recovery ratio (R_r) and shape fixity ratio (R_f) after two shape memory cycles can reach

up to 94.7 % and 95.4 %, respectively. Moreover, the qualitative shape memory property was conducted, a series of deformed shapes can recover its initial strip shape under thermal stimulus (Figure S8, Supporting Information). Fe-IPN can be formed when the IPN film deformed into and fixed at a target shape is immersed into $FeCl_3$ solution due to the swelling ability of IPN (Figure S9, Supporting Information). The inductively coupled plasma (ICP) testing results (Figure S10, Supporting Information) demonstrated that 690 ppm ferric ion was absorbed by IPN during the 5 hours' immersion, which is sufficient to form a stable coordination structure.[37] The amount of ferric ion released from Fe-IPN to water is about 32 ppm after 12 hours' immersion, indicating the stability of Fe-IPN in water. For example, the Fe-IPN with an airplane shape was obtained by immersing an IPN structure with a fixed airplane shape into $FeCl_3$ solution for 5 hours, then it was dried in a vacuum oven for 24 hours.

The formed coordination bond between ferric ion and carboxylic acid provides a crosslinked network, which enables plastic deformation in the IPN. The term "coordination plasticity" used to describe the Fe-IPN structure's shape changing behaviors in this work refers to the capability of a crosslinking structure to undergo permanent deformation enabled by metal coordination that fixes the deformed shape. As a result, the deformed airplane shape is stable. To distinguish the shape memory effect of the coordination interaction-induced Fe-IPN from that of the UPy dimers network, we examined the shape memory property of Fe-IPN at high temperature. The results showed that the Fe-IPN could keep elasticity at a high temperature, whereas IPN underwent plastic deformation due to the dissociation of UPy dimers. The deformed flat film could recover its permanent ferric-coordination airplane shape at 105 °C (Figure 2B). Furthermore, the DMA quantitative results of the shape memory effect indicated that Fe-IPN possessed a good high-temperature shape memory property with R_r of 98 % and R_f of 93 %, respectively. Compared with IPN, the Fe-IPN possessed a higher storage modulus and better thermal stability, which signicantly expands the range of applications.

The DSC and DMA results indicated that the IPN possessed a wide transition temperature area, thus it has the potential for triple shape memory performance.[45] Here, 45 °C and 75 °C were chosen as the two transition temperatures for the triple shape memory process. The combined qualitative and quantitative shape deformation and recovery processes are illustrated in Figure 2C. The initial strip (dyed by rhodamine B) shape (defined as shape 0) was deformed in two steps to temporary shapes ⅰ and ⅱ via triple shape programming. During the shape recovery process, the temporary shape ⅱ could switch to shape ⅰ and then to the initial shape in succession when it was firstly heated at 45 °C and then elevated to 75 °C (Video 2). The quantitative results showed that the Rf (0 to ⅰ) and Rf (ⅰ to ⅱ) of IPN could reach up to 98 % and 93 %, respectively; the Rr (ⅱ to ⅰ) and Rr (ⅰ to 0) could reach up to 97 % and 87 %, respectively. Both the qualitative and quantitative results demonstrated that the IPN has a good triple shape memory effect either under a bending or a stretching mode. We also studied the water-induced shape recovery property of PPT-IPN and Fe-IPN. As shown in Figure S11 and Video 3 and 4, the deformed flat shape could recover its initial helical shape (the helical shape was obtained by thermal plastic deformation and Fe coordination interaction) when immersed into water. This is due to the hydrophilicity of PVA and poly(acrylate acid) segments in the IPN structure. More interestingly, the recovery rate of IPN (80 s) was faster than that of Fe-IPN (150 s). It is because that the coordination interaction consumed some hydrophilic units (carboxyl) from poly (acrylate acid), thus reducing the amount of hydrophilic units of IPN. The IPN structure could shield and stabilize the dimerized UPy motifs with strong hydrogen bonding,[49, 50] resulting in its water-induced shape memory performance.

3.3. Thermadapt Shape Memory Properties of the IPN.

We studied the adaptive plastic deformation of IPN upon thermal stimulation. There exists a reversible dynamic non-covalent bonding from the dissociation and reconfiguration of UPy

dimers under high and low temperature, respectively. As shown in Figure 3, two UPy monomers could form a stable non-

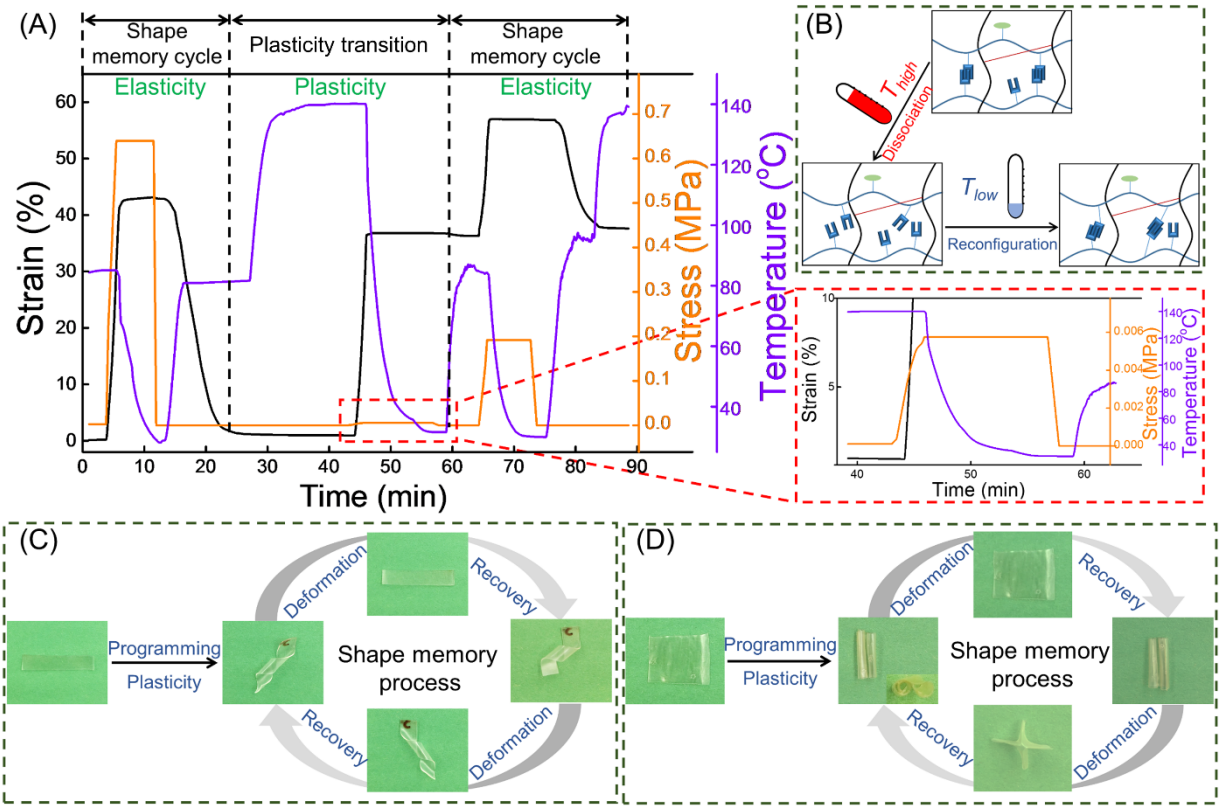

Figure. 3 Thermal plastic deformation process of IPN, and its shape memory process of PPT-IPN (**A**); plastic deformation mechanism of IPN under heating (**B**); plastic deformation process and its shape memory property (**C**) ; plastic deformation process and its shape memory property (**D**).

covalent crosslinking structure, which establishs the basis of the shape memory effect (Figure 3A, left part shape memory cycle of DMA curve). The formed UPy dimers possessed a reversible process between dissociation and recombination. Thus, the IPN has the capability to reconfigure (i.e., via plastic deformation) under high temperature. We studied a shape memory cycle of IPN, the R_r and R_f could reach up to 97 % and 95 %, respectively (Figure 3A). Then the recovered IPN was treated at an elevated temperature (140 °C) for 15 min to completely dissociate the UPy dimers. As shown in the enlarged inset, a large deformation occurred with a quite small force, which was due to the highly soft state of IPN at a high temperature (above its glass transition temperature). Meanwhile, the thermal programmed IPN could complete the reconfiguration by fixing the deformed strain through reducing the temperature under stress and subsequently releasing the applied stress (Figure 3A, middle part plastic deformation of DMA

curve). The shape retention ratio ($R_{ret} = \varepsilon/\varepsilon_{load} \times 100\%$, where ε is the strain of final programmed IPN after releasing the load, ε_{load} is the strain of PPT-IPN under the load.) was introduced to quantify the plasticity transiton;[16] PPT-IPN can hold its length and the R_{ret} can reach up to 96 %, indicating the IPN containing reconfigurable UPy monomers possesses good plastic deformation. For the qualitative process of thermal plasticity, we redefined the shape retention ratio as $R_{ret} = \kappa_n/\kappa_0 \times 100\%$, where κ_n is the curvature of the ring shape obtained from n cycles of thermal plastic deformation (after releasing the applied stress), while κ_0 is the initial curvature of ring shape. The shape retention ratio of PPT-IPN can reach up to 98.5% (n = 1, Figure S12). We investigated the shape memory property of PPT-IPN (Figure 3A, right part shape memory cycle of DMA curve). A temporary deformation could be fixed by cooling the stretched material. The PPT-IPN was stable at room temperature while recovering the shape with plastic length instead of the initial shape (strain is 0). The R_r and R_f could reach up to 97 % and 93 % , respectively. No noticeable deterioration in performance (shape fixing and recovery) was observed after plasticity. The recovered shape was stable under an elevated temperature, indicating the successful plastic deformation. Furthermore, the thermal plastic deformation of IPN provided it with unprecedented flexibility in shape reconfiguration.

Figure 3C shows that a strip could be programmed into a permanent right-handed helical shape under plastic deformation. In the shape memory process, it could exhibit a variety of temporary shapes (a straight strip or a left-handed helical shape), and could recover its programmed right-handed helical shape due to its elasticity (Video 5 and 6). Moreover, complicated origami shapes were obtained by plastic deformation. A square film could be plastically rolled to a permanent scroll shape, which can be fixed to a temporary flat or complex origami structure (Figure 3D), and recovered under high temperature, indicating the good shape memory property of the scroll specimen (Video 7). Videos in the Supporting Information show the shape recovery process of various deformed structures. Owing to the excellent thermadapt shape memory properties, the IPN has potential applications in actuators. For

example, as shown in Figure S13, by heating at 75 ºC for 20 min, the actuator can be deformed into a complex temporary shape to grasp the object, then cooled at 25 ºC to fix the temperature shape. Then, when the actuator was heated to 75 ºC again, the actuator released the object automatically due to the actuator recovering to original shape (Video 8).

3.4. Sequential Adaptive Shape Changing in Different Stimuli.

The sequential adaptive plasticity adds a unique feature for shape programming. Besides thermal plastic deformation, the IPN structure can undergo chemically induced plastic deformation through ferric coordination and

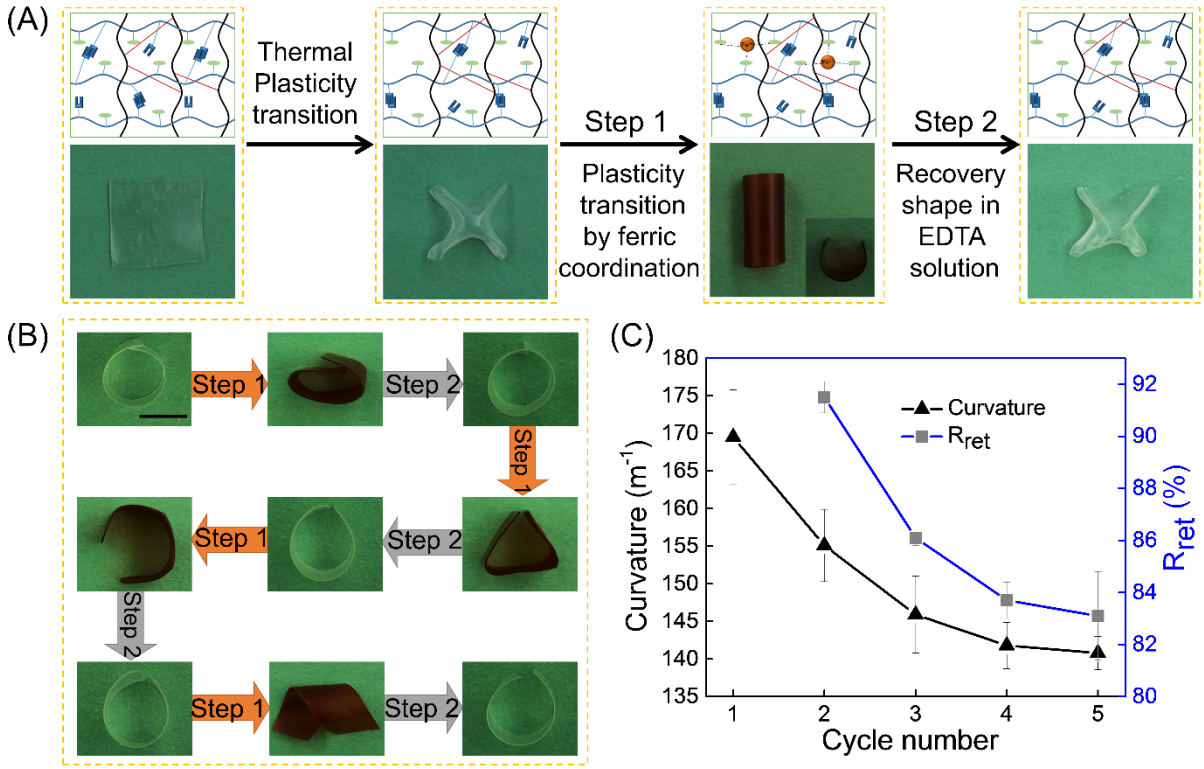

Figure. 4 Sequential plastic deformation upon heating and ferric solution, and the recovery process of Fe-IPN in EDTA solution (**A**); the serializable plastic deformation and recovery process of PPT-IPN in $FeCl_3$ and subsequently EDTA solution (**B**); the effect of cycle number on curvature and R_{ret} of recoveried shape (**C**). Scale bar, 1 cm.

these two types of plastic deformation can occur sequentially to allow for multiple shape changes on demand. Here we studied the sequential plasticity of the IPN upon heating and subsequently immersed in ferric ion solution, defined as T-C (thermal-coordinational) type sequential plasticity. Figure 4 shows that the initially flat film could be plastically deformed into an umbrella shape at high temperature (Fig. 4A), which demonstrated good shape memory effect (Video 9). Then the umbrella shape was deformed to a rolled-up shape at 70 °C, which

was fixed when immersed into 0.5 mol/L $FeCl_3$ solution for 5 hours and dried in a vacuum oven for 24 hours. A stable rolled-up shape with ferric coordination was fabricated. More interestingly, the Fe-IPN could swell to transparent (water uptake: 95%) and back to the first plastic umbrella shape after the treatment by EDTA solution for 24 hours. This phenomenon illustrated that the IPN with thermal plastic deformation exhibited high stability against water. We further investigated the effect of the cycle number of coordination plasticity on the shape retention of the PPT-IPN. Figure 4B shows that a ring shape after thermal plastic deformation could be programmed to a variety of arbitrarily assigned shapes by fixing through ferric coordination (Step 1). These shapes switched back to the original ring shape when incubating Fe-IPN in an EDTA solution for 24 hours (Step 2), resulting from dissociation of the coordination bonding. It illustrated that the PPT-IPN still had stable shape memory effect after five cycles of coordination plasticity on the shape retention. The recovered ring shape was obtained by drying the swelling ring shape in vacuum at RT for 24 hours. We redefined the shape retention ratio as $R_{ret} = \kappa_n/\kappa_0 \times 100\%$, where κ_n is the curvature of ring shape that obtained from n cycles of coordination plastic deformation and EDTA treatment process, κ_0 is the initial curvature of ring shape. In this case, the deformation or shape change is global as compared to the local deformation of folded shapes typically used for testing the shape memory effect. The curvature of the recovered ring shape decreased slightly with increased cycle number, resulting in the decrease of the shape retention ratio (Figure 4C), which still reached up to 83% after five recovery cycles from the coordination plasticity/EDTA treatment. In addition, no noticeable deterioration in performance (shape fixing and recovery ratios) was observed, indicating the thermal plasticity based on the UPy dimers has good stability in water despite the swelling effect.

An interesting question arises- what would happen if the order coordination of the plastic deformation and thermal plastic deformation is switched? In other words, is C-T (coordinational-thermal) type sequential plastic deformation possible? We already found that

Fe-IPN has good shape memory fixity and recovery due to the coordinated plastic deformation (Figure 2B). However, the coordinated IPN could not keep its plastically deformed shape after thermal plastic deformation. This is probably because the coordination crosslinked structure was dissociated after ~20 min thermal treatment when the ferric coordination debonds.[51] Nevertheless, as illustrated in Figure 2B, the Fe-IPN still exhibited good high temperature shape memory effect because the recovery time and temperature of shape memory process were lower than that of the thermal treatment for inducing thermal plasticity. Although for this particular system, first inducing coordination plasticity followed by thermal plastic deformation does not achieve similar multiple shape changes, it might be possible for materials with other reversible group to have the capability of having a C-T type sequential adaptive plastic deformation if the system has a reversible coordination plasticity "switch" that will not be destroyed during the thermal plasticity treatment, which opens ample venues for future research.

4. Conclusions

In summary, we developed a multi-shape-changing IPN system, including thermal, coordination, and sequential plastic deformations. Both IPN and Fe-IPN showed good shape memory property in a wide temerature area. The IPN can be plastically deformed to various structures on demand by virtue of sequential thermal and coordination-induced plastic deformation. Notably, significant shape retention of the PPT-IPN was achieved even after five cycles of repeated coordination plastic deformation and de-coordination. Therefore, this study provides a new route to easily fabricate versatile permanent 3D geometries through programmable plastic deformation and shape memory effects that will find a broad array of applications in actuators, soft robotics, and biomedical devices.

Data availability

The data that support the findings of this study are available from the corresponding authors upon request.

References

1 Reeder, J.T., et al., Adv. Mater., 30 (2018), pp. 1706733
2 Xu, W., K.S. Kwok, and D.H. Gracias, Acc. Mater. Res., 51 (2018), pp. 436-444
3 Boothby, J., H. Kim, and T. Ware, Sens. Actuators B. Chem., 240 (2017), pp. 511-518
4 Medina-Sánchez, M., et al., Adv. Funct. Mater., 28 (2018), pp. 1707228
5 Ning, X., et al., Adv. Mater. Interfaces, 5 (2018), pp. 1800284
6 Zhao, Q., H.J. Qi, and T. Xie, Prog. Polym. Sci., 49-50 (2015), pp. 79-120
7 Wang, Y., et al., Macromol. Chem. Phys., 220 (2018), pp. 1800390
8 Zhao, R., et al., Adv. Mater., 29 (2017), pp. 1605908
9 Huang, L., et al., Adv. Mater., 29 (2017), pp. 1605390
10 Jin, B., et al., Sci. Adv., 4 (2018), pp. eaao3865
11 Wang, B. and M.A. Meyers, Adv. Sci., 4 (2017), pp. 1600360
12 Kirillova, A., et al., Adv. Mater., 29 (2017), pp. 1703443
13 Liu, Y., et al., Sci. Adv., 3 (2017), pp. e1602417
14 Shim, T.S., et al., Nat. Nanotechnol, 12 (2017), pp. 41-47
15 Wu, X., et al., Polymers, 5 (2013), pp. 1169-1202
16 Zhao, Q., et al., Sci. Adv., 2 (2016), pp. e1501297
17 Xia, Y., et al., Adv. Mater., 33 (2021), pp. 2000713
18 Taynton, P., et al., Adv. Mater., 26 (2014), pp. 3938-3942
19 Ji, S., et al., ACS Appl. Mater. Interfaces, 9 (2017)
20 McBride, M., et al., Adv. Mater., 29 (2017), pp. 1606509
21 Zou, W., et al., Adv. Mater., 29 (2017), pp. 1606100
22 Zhang, G., et al., ACS Macro Lett., 5 (2016), pp. 805-808
23 Zheng, N., et al., Angew. Chem., 128 (2016)
24 Zhang, G., et al., Adv. Funct. Mater., 26 (2016), pp. 931-937
25 Liu, D., et al., ACS Macro Lett., 7 (2018), pp. 705-710
26 Yang, L., et al., Angew. Chem. Int. Ed., 56 (2017), pp. 12599-12602
27 Holten-Andersen, N., et al., Proc. Natl. Acad. Sci. U S A, 108 (2011), pp. 2651
28 Foster, E.J., E. Berda, and E. Meijer, J. Am. Chem. Soc., 131 (2009), pp. 6964-6
29 Roy, N., B. Bruchmann, and J.-M. Lehn, Chem. Soc. Rev., 44 (2015)
30 Bosman, A.W., R.P. Sijbesma, and E.W. Meijer, Mater. Today, 7 (2004), pp. 34-39
31 Feldman, K., et al., Macromolecules, 42 (2010)
32 Hummelen, J.C., et al., J. Mater. Chem., 12 (2002)
33 Dankers, P.Y.W., et al., Nat. Mater., 4 (2005), pp. 568-574
34 Wang, F., et al., Angew. Chem. Int. Ed., 49 (2010), pp. 1090-1094
35 Peng, F., et al., J. Am. Chem. Soc., 130 (2008), pp. 16166-16167
36 Lin, P., et al., Adv. Mater., 27 (2015), pp. 2054-2059
37 Zhao, L., et al., Macromol. Mater. Eng., 302 (2017), pp. 1600359
38 Sun, J.-Y., et al., Nature, 489 (2012), pp. 133-136
39 Darabi, M.A., et al., Adv. Mater., 29 (2017), pp. 1700533
40 Ha, S.M., et al., Adv. Mater., 18 (2006), pp. 887-891
41 Zhu, B., et al., Carbohydr. Polym., 133 (2015), pp. 448-455
42 Zheng, J., et al., Mater. Today, (2021) doi.org/10.1016/j.mattod.2021.07.003
43 Kaiser, S., et al., Soft Matter, 15 (2019), pp. 6062-6072
44 Wang, T.X., et al., Polymers, 12 (2020), pp. 2330
45 Xie, T., Nature, 464 (2010), pp. 267-270
46 Zheng, X., et al., Biomaterials, 27 (2006), pp. 4288-4295
47 Zheng, P. and T.J. McCarthy, J. Am. Chem. Soc., 134 (2012), pp. 2024-2027
48 Scott, T., et al., Science, 308 (2005), pp. 1615-7
49 Monemian, S. and L.T.J. Korley, Macromolecules, 48 (2015), pp. 7146-7155

50 Xiao, X.C., et al., Adv. Funct. Mater., 13 (2003), pp. 847-852
51 Shen, P.W., C-Y Jiang, S. X. Sun, J. Zhang, Electrochem. Energy, (2015), pp. 405-420

Acknowledgements

Z. Chen acknowledges the startup fund from the Thayer School of Engineering at Dartmouth and the support from the Branco Weiss–Society in Science Fellowship, administered by ETH Zürich. J. Fan acknowledges the support from ACS Petroleum Research Fund and CUNY Advanced Science Research Center. This work was partially supported by the National Natural Science Foundation of China (Grant Nos. 51603172 and 51725303). The author thanks the help of DSC and DMA characterizations from Materials Research Science and Engineering Center in Harvard (DMR-1420570).

Author contributions

L.W. and S. W. contributed equally to this work.
L.W. and Z.C. conceived the concept and supervised the project. L.W., S. W., X.G, J.F., S.Z. and Z.C. designed the experiments and wrote the manuscript. L.W. performed the experiments. Experimental results were collected and analyzed through contributions of all authors.

Additional information

Supplementary Information

Competing interests: The authors declare no competing interests.